

# Flatband Engineering of Mobility Edges

Carlo Danieli,<sup>1</sup> Joshua D. Bodyfelt,<sup>1</sup> and Sergej Flach<sup>1,2</sup>

<sup>1</sup>*New Zealand Institute for Advanced Study, Centre for Theoretical Chemistry & Physics, Massey University, Auckland, New Zealand*

<sup>2</sup>*Center for Theoretical Physics of Complex Systems, Institute for Basic Science, Daejeon, Korea*

Properly modulated flatband lattices have a divergent density of states at the flatband energy. Quasiperiodic modulations are known to host a metal insulator transition already in one space dimension. Their embedding into flatband geometries consequently allows for a precise engineering and fine tuning of mobility edges. We obtain analytic expressions for singular mobility edges for two flatband lattice examples. In particular, we engineer cases with arbitrarily small energy separations of mobility edge, zeroes, and divergencies.

PACS numbers: 71.10.-w, 71.30.+h, 72.20.Ee

## I. Introduction

The phenomenon of wave localization has been intensively studied since its prediction in 1958 [1], where complete localization was proved in the case of a one-dimensional (1-D) chain defined over a random potential. Moreover, it was shown that the 3-D case allows for an energy-dependent transition from localized to delocalized eigenstates. The transition has been since coined metal-insulator transition (MIT). The critical energy  $E_c$  is called a mobility edge; in general, it depends on and varies upon changes of the control parameters of the given model [2]. Interestingly, an MIT can also be realized in one-dimensional settings with sufficiently correlated disorder potentials [3].

In 1980, Aubry and André proved the existence of the MIT for a 1-D chain defined over a specific quasiperiodic potential [4]. This MIT occurs at a critical value ( $\lambda_c = 2$ ) of the onsite potential's strength  $\lambda$ , and separates the metallic phase  $\lambda \in ]0, 2[$  from an insulating phase  $\lambda \in ]2, +\infty[$ . This remarkable result was fully understood via the principle of duality, in which a particular Fourier transformation relating eigenmodes and energy spectra allows for a direct functional equivalency between momentum space and its transform counterpart. This equivalency is energy-independent: upon crossing the critical value  $\lambda_c$  all eigenstates turn from localized to extended, regardless of their eigenenergy. The appearance of a mobility edge is thus avoided. Analytic results have been discovered in the last decade regarding the topological Cantor structure of the spectrum [5] and its Lebesgue measure [6]. Furthermore, for each different regime (insulating, metallic and critical) different spectral decompositions have been found [7–9]. Model generalizations were reported, e.g. quasiperiodic systems constantly maintained at criticality [10, 11], bichromatic quasiperiodic lattices displaying mobility edges [12, 13], and completely localized quasiperiodic models [14]. Correlated metallic states have also been observed in the insulating regime, for the case of two interacting particles within a 1-D Aubry-André chain [15]. In another recent work [16], a suitably modified quasiperiodic potential was

shown to produce a mobility edge expressible in an analytic form - a property which we will take to new limits using flatband topologies.

Wave propagation on lattices with flatband topologies is characterized by the existence of horizontal (flat) bands in their band structure. Known in condensed matter, this model class has gained great interest in the scientific community, due in part to experimental realizations in optical lattices and paraxially approximate light propagations [17–19]. Recent theoretical discoveries have also considered the presence of a disordered potential [20, 21] and nonlinearity [22]. An innovative procedure detangles flatband states from dispersive ones [23]. This allows one to inspect specific features of the models as they relate to the choice of the onsite perturbations, and also suggests specific potential correlations. In the present work, this detangling technique of local rotations [23] is applied as an extension of [24]; in particular, regarding the preliminary finding of a MIT occurring in a flatband lattice under quasiperiodic Aubry-André perturbation.

The present paper has the following structure: in Sec. II the general features of flatband topologies are introduced that define two particular models (cross-stitch and diamond lattices), a quasiperiodic Aubry-André onsite perturbation is defined, and the coordinate transformation that allows rotation into Fano defect lattices [23]. In Sec. III-IV, our findings for the cross-stitch and diamond lattices are respectively presented: for both, two distinct chain correlations are discussed. Where applicable, the exact mathematical expression obtained for the mobility edge is jointly shown with numerically obtained transitions for these particular onsite correlations.

## II. Flatband Topologies

Consider the eigenvalue problem of a generalized tight-binding model

$$E\psi_n = \epsilon_n\psi_n - \hat{V}\psi_n - \hat{T}(\psi_{n-1} + \psi_{n+1}). \quad (1)$$

For all  $n \in \mathbb{Z}$ , each component of the vector  $\psi_n = (\psi_n^1, \dots, \psi_n^\ell)^T$  represents a site of a periodic lattice, while

the set of sites represented by  $\psi_n$  is the  $n$ -th unit cell. The real matrix  $\hat{V}$  defines the geometry of the unit cell, while the real matrix  $\hat{T}$  describes hopping to neighboring cells. At each of the lattice's  $i$ -th leg  $\{\psi_n^i\}_n$ , an onsite perturbation  $\{\epsilon_n^i\}_n$  is defined. The unit cell perturbation  $\epsilon_n$  of Eq.(1) is thus given by the diagonal square matrix  $\epsilon_n = \text{diag}(\epsilon_n^a, \epsilon_n^b, \dots, \epsilon_n^\ell)$ .

The model geometry is contained in the matrices  $\hat{T}$  and  $\hat{V}$ , which are then used to derive the dispersion spectrum via the Bloch solution  $\psi_n = \phi_k e^{ikn}$  on an unperturbed crystal  $\epsilon_n = 0$ . Flatband topologies are models in which this crystalline case exhibits *at least* one band independent of  $k$  – such a band is dispersionless, or “flat”. Eigenmodes corresponding to this flatband energy are (usually) compact localized states (CLS), *i.e.* modes whose amplitude is nonzero only across a finite number of sites [23]. The flatband topology class,  $U$ , is then defined as the minimum number of unit cells the CLS occupies [23].

In this paper we consider two lattice topologies – the cross-stitch and diamond lattices. The former, shown in the upper left of Fig.1, is defined for a unit cell  $\psi_n = (a_n, b_n)^T$  with a  $2 \times 2$  perturbation matrix  $\epsilon_n$ . This yields for Eq.(1) the following matrices

$$\hat{V}_{CS} = \begin{pmatrix} 0 & t \\ t & 0 \end{pmatrix}, \quad \hat{T}_{CS} = \begin{pmatrix} 1 & 1 \\ 1 & 1 \end{pmatrix}. \quad (2)$$

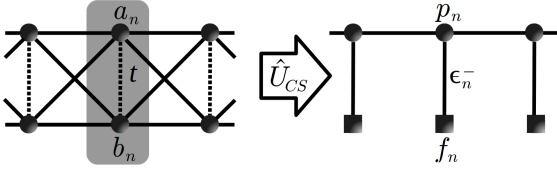


FIG. 1. Left: The cross-stitch lattice – the grey shaded region indicates the unit cell. Right: The transformed Fano defect lattice of Eq.(9).

Likewise for the diamond lattice, as shown in the upper left of Fig.2, the unit cell is  $\psi_n = (a_n, b_n, c_n)^T$  with a  $3 \times 3$  perturbation matrix  $\epsilon_n$ . In this case, the matrices in Eq.(1) are

$$\hat{V}_{DC} = \begin{pmatrix} 0 & t & 1 \\ t & 0 & 1 \\ 1 & 1 & 0 \end{pmatrix}, \quad \hat{T}_{DC} = \begin{pmatrix} 0 & 0 & 0 \\ 0 & 0 & 0 \\ 1 & 1 & 0 \end{pmatrix}. \quad (3)$$

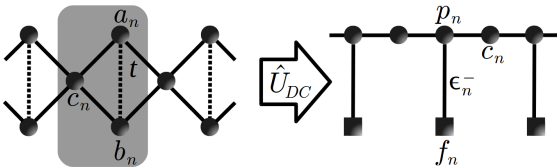


FIG. 2. Left: The diamond lattice – the grey shaded region indicates the unit cell. Right: The transformed Fano defect lattice of Eq.(20).

In the unperturbed crystal  $\epsilon_n = 0$ , the dispersive bands are

$$E(k) = \begin{cases} -t - 4 \cos k, & \text{Cross-Stitch,} \\ -\frac{1}{2} (t \pm \sqrt{t^2 + 16 \cos k + 16}), & \text{Diamond.} \end{cases}$$

Additionally, both models contain a flat band at  $E(k) = t$ .

Associated with the flatband energy, a resulting CLS can be constructed:  $\psi_n = (1, -1)^T \delta_{n,n_0} / \sqrt{2}$  (cross-stitch) and  $\psi_n = (1, -1, 0)^T \delta_{n,n_0} / \sqrt{2}$  (diamond). Note that both CLS are contained within a single unit cell. Therefore, according to the definition previously stated, both lattices are flatband models class  $U = 1$ . Coordinate transformations local to the unit cells rotate these lattices into a Fano defect form [23]. For the cross-stitch, the rotation is defined by the real matrix  $\hat{U}_{CS}$

$$\begin{pmatrix} p_n \\ f_n \end{pmatrix} = \hat{U}_{CS} \psi_n, \quad \hat{U}_{CS} = \frac{1}{\sqrt{2}} \begin{pmatrix} 1 & 1 \\ 1 & -1 \end{pmatrix}. \quad (4)$$

Similarly for the diamond lattice the transformation is defined by the real matrix  $U_{DC}$

$$\begin{pmatrix} p_n \\ f_n \\ c_n \end{pmatrix} = \hat{U}_{DC} \psi_n, \quad \hat{U}_{DC} = \frac{1}{\sqrt{2}} \begin{pmatrix} 1 & 1 & 0 \\ 1 & -1 & 0 \\ 0 & 0 & \sqrt{2} \end{pmatrix}. \quad (5)$$

Lastly, this local coordinate transformation must also rotate the onsite perturbation. For both lattices, this gives

$$\epsilon_n^\pm = (\epsilon_n^a \pm \epsilon_n^b) / 2. \quad (6)$$

The effect of quasiperiodic Aubry-André perturbations on these two topologies is the focus of the present work. For both lattices, the onsite perturbations  $\{\epsilon_n^i\}$  are defined as *independent* Aubry-André potentials

$$\epsilon_n^i = \lambda_i \cos [2\pi (\alpha n + \theta_i)] , \quad (7)$$

for the  $i = a, b$  (cross-stitch) and  $i = a, b, c$  (diamond) legs. The parameters  $\lambda_i$  are positive real values controlling the perturbative strength,  $\theta_i$  is the phase-shift, and  $\alpha$  is an irrational number (here set to the golden ratio) called the *incommensurate parameter*. Without loss of generality, the  $a$ -leg phase can be zeroed ( $\theta_a = 0$ ). We also set the leg potential strengths equal to each other  $\lambda_i = \lambda$ .

From Eq.(6), notable correlations between the  $a$ -leg and  $b$ -leg perturbations appear and will be object of our studies for both models; namely

$$\begin{aligned} \text{Symmetric: } \epsilon_n^- = 0 &\Leftrightarrow \epsilon_n^a = \epsilon_n^b, \\ \text{Antisymmetric: } \epsilon_n^+ = 0 &\Leftrightarrow \epsilon_n^a = -\epsilon_n^b. \end{aligned} \quad (8)$$

Since the  $a$ -leg phase has been zeroed, from Eq.(7) these two correlations are obtained solely from the  $b$ -leg phase, e.g.  $\theta_b = 0.5$  ( $\theta_b = 0$ ) for the antisymmetric (symmetric) case. We start the analysis of these models with the cross-stitch in Sec.III, and then with the diamond lattice in Sec.IV.

### III. Cross-Stitch Lattice

By Eqs.(4,6), the cross-stitch lattice transforms into

$$\begin{aligned} (E+t)p_n &= \epsilon_n^+ p_n + \epsilon_n^- f_n - 2(p_{n-1} + p_{n+1}), \\ (E-t)f_n &= \epsilon_n^+ f_n + \epsilon_n^- p_n. \end{aligned} \quad (9)$$

This results in a Fano chain, as shown in the right of Fig.1. The local rotation yields a dispersive coordinate  $p_n$  and a compact Fano coordinate  $f_n$ . The sequence  $\epsilon_n^+$  describes onsite perturbations of both  $p_n$  and  $f_n$ , while the sequence  $\epsilon_n^-$  couples the dispersive to the Fano coordinate within the rotated unit cell [23]. Solving for the Fano coordinates  $f_n$  in the second equation above, we obtain a new equation for the dispersive portion

$$(E+t)p_n = \left[ \epsilon_n^+ + \frac{(\epsilon_n^-)^2}{(E-t) - \epsilon_n^+} \right] p_n - 2(p_{n-1} + p_{n+1}). \quad (10)$$

The reduced topology assumes the tight-binding form. If eigenmodes are exponentially localized, their asymptotic decay is  $\psi_n^\nu \sim e^{-\frac{n}{\xi}}$ . The rate  $\xi^{-1}(E)$  is the inverse localization length of a localized state at eigenenergy  $E \in \mathbb{R}$ , found by applying the recursive iteration

$$\xi^{-1}(E, \lambda) = \lim_{M \rightarrow +\infty} \frac{1}{M} \sum_{n=1}^M \ln \left| \frac{p_{n+1}}{p_n} \right|. \quad (11)$$

for any given potential strength  $\lambda$ . We will use this method in all the numerical computations of the two models' localization lengths, for  $M = 10^6$ . The energy  $E$  in Eq.(10) will be numerically found from an exact diagonalization of a finite lattice of  $N = 512$  unit cells. In all the figures of the paper, if the recursive iteration converges to a finite value (chosen [25] here as  $\xi \leq N/10$ ), the datapoint  $(E, \lambda)$  is declared a localized state and plotted in blue. Otherwise if the iteration diverges, the datapoint is declared an extended state and plotted in red.

#### A. Symmetric Case: Metal-Insulator Transition

We analyze first the symmetric case  $\epsilon_n^- = 0$ , obtained for  $\theta_b = 0.0$ . Eq.(9) reads

$$\begin{aligned} (E+t)p_n &= \epsilon_n^+ p_n - 2(p_{n-1} + p_{n+1}), \\ (E-t)f_n &= \epsilon_n^+ f_n \end{aligned} \quad (12)$$

with  $\epsilon_n^+ = \epsilon_n^i$ . The two sets of states  $p_n$  and  $f_n$  decouple and generate two independent spectra, respectively labeled  $\sigma_p$  and  $\sigma_f$ . The parameter  $t$  then simply operates as a shift parameter, translating  $\sigma_p$  and  $\sigma_f$  relative to each other by  $2t$ .

The dispersive states  $p_n$  are described by an Aubry-André chain, displaying a MIT at  $\lambda_c = 4$ . The  $\sigma_f$  states keep their compact feature, but the degeneracy of their eigenenergies is now removed - these eigenenergies are given by  $E = \epsilon_n^+ + t$ . In Fig.3, we plot the spectrum from Eq.(12), as a function of  $\lambda$ . In this symmetric case, the

spectra  $\sigma_p$  and  $\sigma_f$  are independent, since the  $p_n$  and the  $f_n$  coordinates decouple.

For every potential strength  $\lambda > 0$ , the Fano states spectrum  $\sigma_f = \{\epsilon_n^+\}_n$  is equidistributed within the interval  $[t - \lambda, t + \lambda]$ . In Fig.3 we indicate its boundaries by dashed lines. For the dispersive spectrum  $\sigma_p$ , the localization length is numerically found with the recursive iteration (11), and the localized phase (red) is demarcated from the extended one (blue). At the critical value  $\lambda_c = 4$ , all dispersive states switch from extended to localized. In this case, there is no mobility edge.

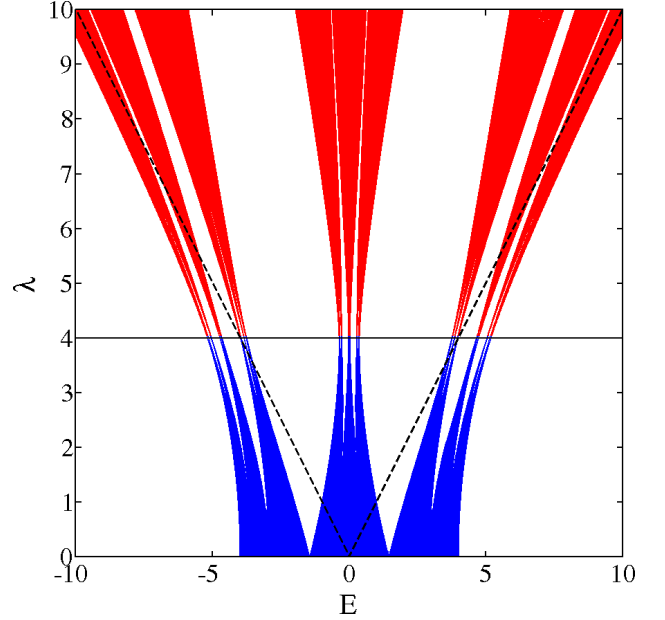


FIG. 3. Symmetric Case: The dispersive spectrum ( $\sigma_p$ ) of the cross-stitch lattice, for  $\epsilon_n^- = 0$  and  $t = 0$ . The Fano state spectrum  $\sigma_f$  is omitted, but its boundaries indicated by black dashed lines. The black line represents the MIT at  $\lambda = 4$ , which clearly separates extended states (blue) from those localized (red).

#### B. Asymmetric Case $\epsilon_n^- \neq 0$ : Numerical Evidence for Mobility Edge

Breaking the symmetry  $\epsilon_n^- \neq 0$  ( $\theta_b \neq 0$ ) of the Fano chain Eq.(9) effectively couples the dispersive states  $p_n$  to their compact Fano counterparts  $f_n$ . Therefore, the self-duality is lost, and the two independent spectra ( $\sigma_{p,f}$ ) are now joint. Nevertheless, we expect a transition between localized and extended states via an energy-dependent mobility edge. In Fig.4 we plot the spectrum of the lattice in the asymmetric case for  $\theta_b = 0.25$  and  $t = 0$ . A mobility edge is clearly observed separating the localized regime (red) from that which is extended (blue).

#### C. Antisymmetric Case ( $\epsilon_n^+ = 0$ ): Analytic Mobility Edge

Among all the possible non-symmetric cases obtained for  $\theta_b \neq 0$ , the antisymmetric one  $\theta_b = 0.5$  deserves spe-

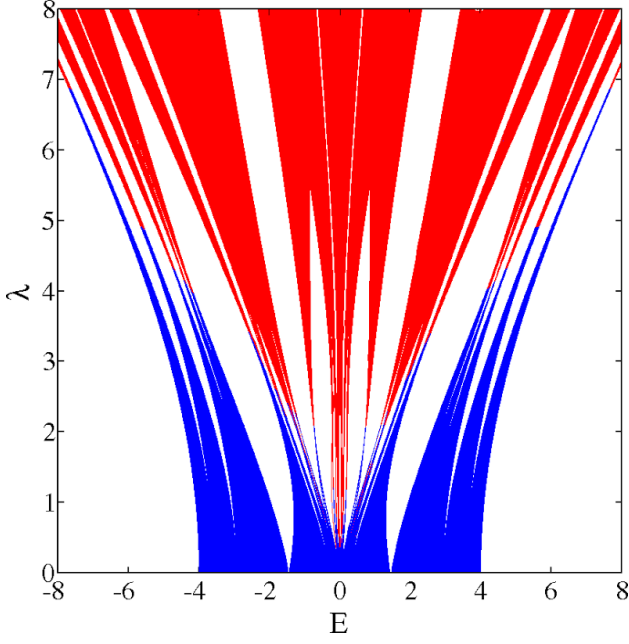


FIG. 4. Asymmetric Case: Spectrum of the cross-stitch lattice, for  $\theta = 0.25$  and  $t = 0$ . The extended (localized) portion of the spectrum is shown in blue (red), while the color boundary is a mobility edge approximation of the spectrum.

cial attention. In this situation  $\epsilon_n^+ = 0$  and Eq.(9) transforms into

$$\begin{aligned} (E+t)p_n &= \epsilon_n^- f_n - 2(p_{n-1} + p_{n+1}), \\ (E-t)f_n &= \epsilon_n^- p_n. \end{aligned} \quad (13)$$

It follows that all flatband states are expelled from their unperturbed energy position  $E = t$ . Since  $\epsilon_n^- \neq 0$ , from the second equation of (13) it follows that at the flatband energy

$$\epsilon_n^- p_n = 0 \quad \Rightarrow \quad p_n = 0, \quad (14)$$

Then, from the first equation of (13) we conclude

$$\epsilon_n^- f_n = 0 \quad \Rightarrow \quad f_n = 0. \quad (15)$$

Only the trivial state  $(p_n, f_n) = (0, 0)$  satisfies Eq.(13) exactly at the flatband energy  $E = t$ . In Fig.5 we plot the spectrum for this antisymmetric case for  $t = 0$ . We again observe a mobility edge. However, we can now even identify its analytical form, as observed in [24]. Indeed the dispersive part, Eq.(10), reads

$$(E+t)p_n = \frac{(\epsilon_n^-)^2}{E-t} p_n - 2(p_{n-1} + p_{n+1}). \quad (16)$$

By trigonometric bisection

$$(\epsilon_n^-)^2 = \lambda^2 \cos^2(2\pi\alpha n) = \frac{\lambda^2}{2} [1 + \cos(4\pi\alpha n)]. \quad (17)$$

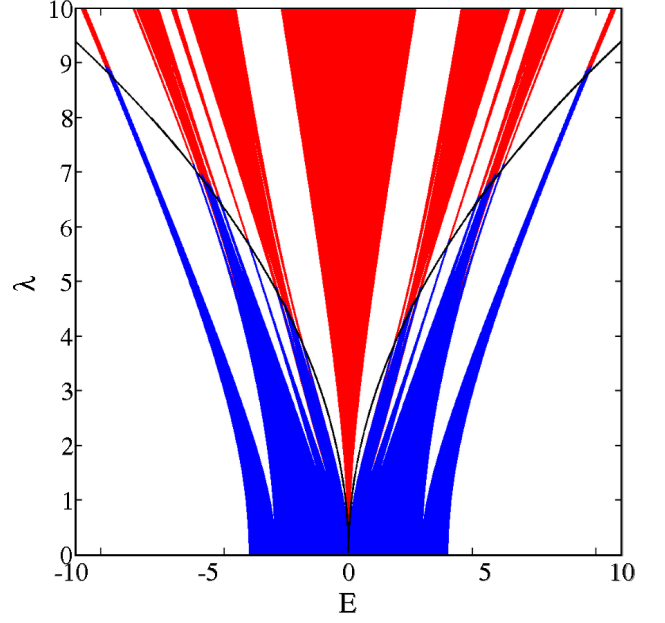


FIG. 5. Antisymmetric Case: Spectrum of the cross-stitch lattice, for  $\epsilon_n^+ = 0$  and  $t = 0$ . The extended (localized) spectral portion is shown in blue (red). The color boundary is an approximation to the spectral mobility edge, however the black line is the analytical form of Eq.(19) – a good agreement is observed.

Substituting Eq.(17) back into the previous equation, we obtain

$$\begin{aligned} \tilde{E} p_n &= \frac{\lambda^2}{4(E-t)} \cos(4\pi\alpha n) - (p_{n-1} + p_{n+1}), \\ \text{where } \tilde{E} &:= \frac{E+t}{2} - \frac{\lambda^2}{4(E-t)}. \end{aligned} \quad (18)$$

Therefore, the model becomes an Aubry-André chain eigen-equation, but with onsite perturbation strength depending on  $\lambda$  and  $E$ . From [4], the MIT occurs when the potential strength is twice larger than the hopping strength. Imposing that condition, an analytic expression is found for the mobility edge,  $\lambda_c(E_c)$ :

$$\left| \frac{\lambda_c^2}{4(E_c-t)} \right| = 2 \quad \Rightarrow \quad \lambda_c(E_c) = 2\sqrt{2|E_c-t|}. \quad (19)$$

Note that for  $E_c = t$ , the critical potential strength  $\lambda_c$  vanishes in a square root manner, where the previously discussed lack of states at the flatband energy  $E = t$  occurs. The analytic curve of the mobility edge is plotted in Fig.5, displaying excellent agreement with the numerical result.

#### IV. Diamond Lattice

Under Eqs.(5, 6), the diamond lattice's Eq.(1) become

$$\begin{aligned} (E+t)p_n &= \epsilon_n^+ p_n + \epsilon_n^- f_n - \sqrt{2}(c_n + c_{n+1}), \\ (E-t)f_n &= \epsilon_n^+ f_n + \epsilon_n^- p_n, \\ (E-\epsilon_n^c)c_n &= -\sqrt{2}(p_{n-1} + p_n), \end{aligned} \quad (20)$$

as illustrated graphically in the right plot of Fig.2.

Expressing the  $f_n$  and  $c_n$  variables through the  $p_n$  ones we reduce these equations to a tight-binding form which contains the  $p_n$  coordinates only:

$$(E+t)p_n = \left[ \epsilon_n^+ + \frac{(\epsilon_n^-)^2}{(E-t)\epsilon_n^+} + \frac{2}{E-\epsilon_n^c} + \frac{2}{E-\epsilon_{n+1}^c} \right] p_n + \frac{2}{E-\epsilon_n^c} p_{n-1} + \frac{2}{E-\epsilon_{n+1}^c} p_{n+1}. \quad (21)$$

We use this tight-binding form to numerically obtain the eigenvalue spectrum and consequently the localization length using the iterative recursion Eq.(11). In Fig.6, we plot the diamond lattice spectrum and the mobility edge for  $\theta_b = 0.5$ ,  $\theta_c = 0.05$  and  $t = 0$ .

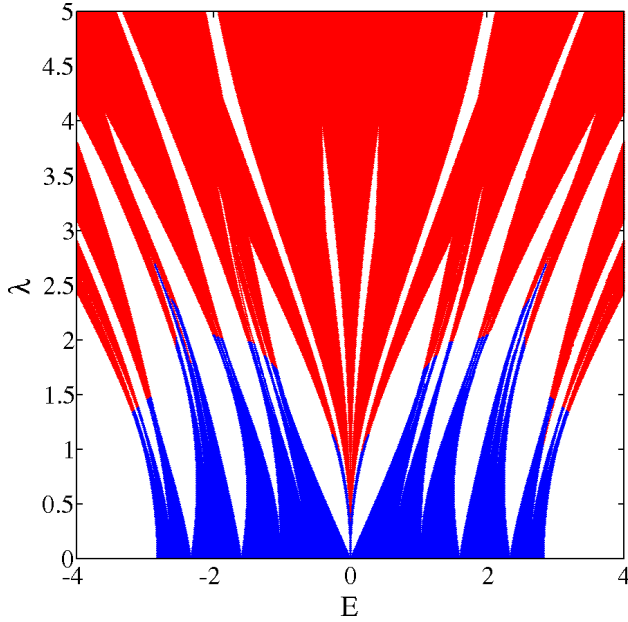


FIG. 6. Spectrum of the diamond lattice, for  $\theta_b = 0.5$ ,  $\theta_c = 0.05$  and  $t = 0$ . The extended (localized) spectral portion is shown in blue (red), while the color boundary is again a spectral mobility edge approximation.

We notice that in Eq.(21) the coefficients of the hopping terms depend on the  $c$ -chain onsite perturbation  $\epsilon_n^c$ . Therefore, in general all hopping terms are perturbation-dependent. In order to arrive at an Aubry-André form of Eq.(21) we set constant onsite energies on all  $c$  sites:  $\epsilon_n^c = K \in \mathbb{R}$ . Then an extended state  $\mathcal{D}$  exists at energy  $E = K$ , regardless of the other control parameters

in Eq.(20):

$$E = K, \quad c_n = (-1)^n, \quad f_n = p_n = 0. \quad (22)$$

The state's amplitudes reside only on the  $c$  sites (see Fig.7). The existence of this extended state is not af-

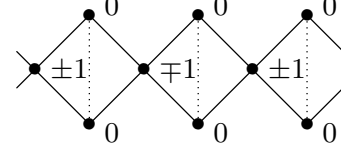


FIG. 7. Extended state  $\mathcal{D}$  at energy  $E = K$  on the diamond lattice in case of constant onsite potential  $\epsilon_n^c = K$  on the  $c$ -chain (up to normalization).

ected by the perturbation strength  $\lambda$ , the flatband energy  $E = t$ , and any specific correlation of the onsite potential. Therefore if the model admits a mobility edge curve  $\lambda_c(E_c)$ , it follows that it will diverge  $\lambda_c(E_c = K) = \infty$ , yielding a singularity.

##### A. Symmetric Case: Analytic Mobility Edge

We consider first the symmetric case  $\epsilon_n^- = 0$ , obtained for  $\theta_b = 0.0$ . In this situation, Eq.(20) reads

$$\begin{aligned} (E+t)p_n &= \epsilon_n^+ p_n + -\sqrt{2}(c_n + c_{n+1}), \\ (E-t)f_n &= \epsilon_n^+ f_n, \\ (E-K)c_n &= -\sqrt{2}(p_{n-1} + p_n). \end{aligned} \quad (23)$$

The  $f_n$  states decouple from both  $p_n$  and  $c_n$  states, generating two independent spectra  $\sigma_f$  and  $\sigma_{p,c}$ . The flatband energy  $t$  shifts the two energy spectra of  $2t$  relative to each other. Substituting the  $c$  variables by the  $p$  ones we obtain the Aubry-André form

$$\tilde{E} p_n = \frac{(E-K)\lambda}{2} \cos(2\pi\alpha n) p_n + p_{n-1} + p_{n+1},$$

$$\text{where } \tilde{E} := \frac{(E+t)(E-K)}{2} - 2. \quad (24)$$

Note the onsite potential strength is now dependent on  $\lambda$  and  $E$ . Imposing the equality between the potential strength and the Aubry-André critical value, we arrive at the mobility edge

$$\left| \frac{(E_c - K)}{2} \lambda_c \right| = 2 \quad \Rightarrow \quad \lambda_c(E_c) = \left| \frac{4}{E_c - K} \right|. \quad (25)$$

The mobility edge curve diverges at  $E = K$  due to the existence of the delocalized state  $\mathcal{D}$ . We plot this mobility edge curve in Fig.8 and observe very good agreement with the numerical results.

##### B. Antisymmetric Case: Analytic Mobility Edge

We consider the antisymmetric case  $\epsilon_n^+ = 0$  obtained with  $\theta_b = 0.5$ , and with  $\epsilon_n^c = K$ . Eq.(20) reads

$$\begin{aligned} (E+t)p_n &= \epsilon_n^- f_n - \sqrt{2}(c_n + c_{n+1}), \\ (E-t)f_n &= \epsilon_n^- p_n, \\ (E-K)c_n &= -\sqrt{2}(p_{n-1} + p_n). \end{aligned} \quad (26)$$

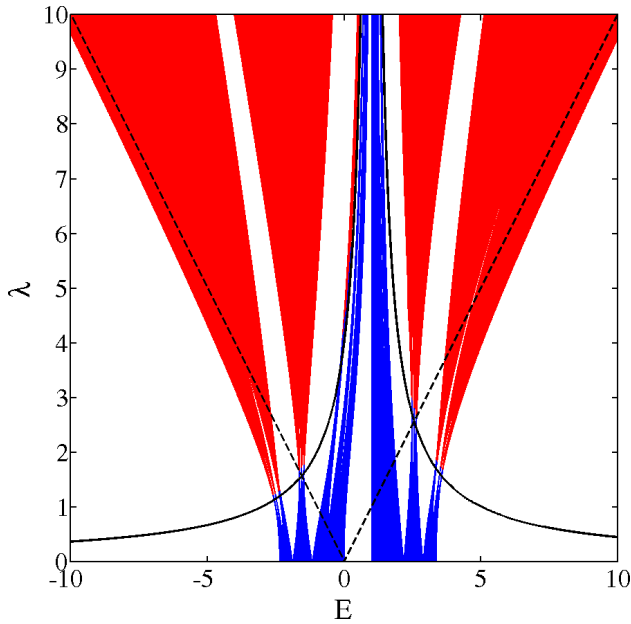


FIG. 8. Symmetric Case: Dispersive spectrum ( $\sigma_{p,c}$ ) of the diamond lattice, for  $\epsilon_n^+ = 0$ ,  $K = 1$ ,  $t = 0$ . The Fano state spectrum ( $\sigma_f$ ) is omitted, but its boundaries are indicated by black dashed lines. The extended (localized) states of the dispersive spectrum are shown in blue (red) – the boundary between these is a mobility edge approximation, in good agreement with its analytical form of Eq.(25), shown as a solid black line. Note that at  $E = K$ , the mobility edge diverges to infinity.

For  $t \neq K$ , all eigenenergies are expelled from the flatband energy  $E = t$ . In Fig.9 we plot the spectrum for this antisymmetric case for  $t = -1$  and  $K = 1$ . We derive an analytical expression of the mobility edge by reducing Eq.(26) to an Aubry-André form for the  $p_n$  coordinates:

$$\tilde{E} p_n = \frac{E - K}{2} \frac{\lambda^2}{2(E - t)} \cos(4\pi\alpha n) p_n + p_{n-1} + p_{n+1},$$

where  $\tilde{E} := \frac{E - K}{2} \left[ (E + t) - \frac{\lambda^2}{2(E - t)} \right] - 2$ . (27)

The condition for the MIT yields

$$\left| \frac{E - K}{2} \frac{\lambda_c^2}{2(E - t)} \right| = 2 \Rightarrow \lambda_c(E) = 2\sqrt{2 \left| \frac{E - t}{E - K} \right|} \quad (28)$$

In Eq.(28), the mobility edge curve  $\lambda_c(E_c)$  diverges to infinity at  $E = K$ , in correspondence to the delocalized state  $\mathcal{D}$ . The curve also displays a zero at  $E = t$ , which corresponds to the lack of any states at the flatband energy [26]. The mobility edge curve of Eq.(28) is plotted in Fig.9 and show excellent agreement with the numerical data.

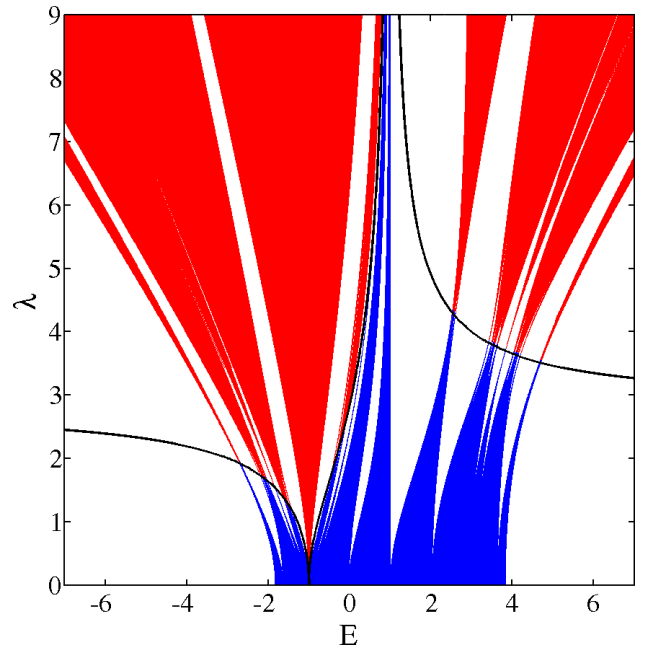


FIG. 9. Antisymmetric Case: Spectrum of the diamond lattice, for  $\epsilon_n^+ = 0$ ,  $K = 1$ ,  $t = -1$ . The extended (localized) spectral portion is shown in blue (red). The boundary between is an approximation of the spectrum's mobility edge – in good agreement with the analytical form of Eq.(28), plotted as a black line. Note the mobility edge curve zeroes at  $E = t$ , as well as diverges at  $E = K$ .

## V. Conclusion

Flatband topologies are characterized by macroscopic degeneracy at the flatband energy. General perturbations of these topologies lead to a removal of the degeneracy, yet keeps a high density of states and a bunching of the renormalized and hybridized states around the original flatband energy. This has especially dramatic consequences for quasiperiodic Aubry-André form perturbations. The flatband energy now hosts a zero of a mobility edge curve  $\lambda_c(E_c)$ . When approaching this zero the density of states grows, and the spatial extent of the eigenstates drops, making them more localized. For specific symmetries of the applied quasiperiodic potential, the dependence  $\lambda_c(E_c)$  is obtained analytically, confirming the predicted zero, and further proving the strict nonexistence of any state at the former flatband energy. Some flatband topologies allow the existence of completely delocalized eigenstates at certain energies  $E = K$ . This leads to even more complex mobility edge curves which allow for a coexistence of zeroes and divergencies of  $\lambda_c(E_c)$ . Possible future topics of study include extension to  $U > 1$  topological classes and higher dimensional flatband models. It is our hope that the use of flatband topologies contributes interest to tunable mobility edges, e.g. by those realized in graphene [27], monolayered dichalcogenides [28], or vanadium dioxide films [29].



- 
- [1] P. W. Anderson, Phys. Rev. **109**, 1492 (1958). (1958).
  - [2] B.R. Bulka, B. Kramer and A. MacKinnon, Z. Phys. B - Condensed Matter **60**, 13-17 (1985).
  - [3] F. Izrailev and A. A. Krokhin, Phys. Rev. Lett. **82**, 4062 (1999).
  - [4] S. Aubry and G. Andre, Ann. Israel Phys. Soc., vol. 3, Hilger, Bristol, 1980, pp. 133-164
  - [5] A. Avila and S. Jitomirskaya, Annals of Mathematics **170**, 303 (2009).
  - [6] S. Jitomirskaya and I. V. Krasovsky, Math. Res. Lett. **9**, 413 (2002).
  - [7] A. Avila, arXiv:0810.2965 (2008).
  - [8] S. Jitomirskaya, Ann. of Math. **150** 1159 (1999).
  - [9] A. Gordon, S. Jitomirskaya, Y. Last and B. Simon, Acta Math **178**, 169 (1997).
  - [10] S. Ostlund, R. Pandit, D. Rand, H. J. Schellnhuber and E. D. Siggia, Phys. Rev. Lett. **50**, 1873 (1983).
  - [11] M. Kohmoto, L. P. Kadanoff and C. Tang, Pys. Rev. Lett. **50**, 1870 (1983).
  - [12] H. Hiramoto and M. Kohmoto, Phys. Rev. B **40**, 8225 (1989).
  - [13] D.J. Boers, B. Goedeke, D. Hinrichs, M. Holthaus, PRA **75**, 063404 (2007).
  - [14] D. R. Grempell, S. Fishman and R. Prange, Phys. Rev. Lett. **49**, 833 (1982).
  - [15] S. Flach, M. Ivanchenko and R. Khomeriki, EPL **98**, 66002 (2012).
  - [16] S. Ganeshan and S. Das Sarma, arXiv: 1411.7375v1.
  - [17] F. Bloch, J. Dalibard and W. Zwerger, Rev. Mod. Phys. **80**, 885 (2005).
  - [18] D.N. Christodoulides, F. Lederer and D. Silberberg, Nature **424**, 817 (2003).
  - [19] N. Masumoto, N. Kim, T. Burnes, K. Kusudo, A. Loefler, S. Hoefling, A. Forchel and Y. Yamamoto, New. J. Phys. **14**, 065002 (2012).
  - [20] O. Derzhko and J. Richter, Eur. Phys. J. B **52**, 23 (2006).
  - [21] O. Derzhko, J. Richter, A. Honecker, M. Maksymenko, and R. Moessner, Phys. Rev. B **81**, 014421 (2010).
  - [22] D. Leykam, S. Flach, O. Bahat-Treidel O. and A.s. Desyatnikov, Phys. Rev. B **88**, 224203 (2013).
  - [23] S. Flach, D. Leykam, J. D. Bodyfelt, P. Matthies, and A. S. Desyatnikov, Europhys. Lett. **105**, 30001 (2014); *ibid*, **106**, 19901 (2014).
  - [24] J.D. Bodyfelt, D. Leykam, C. Danieli, X. Yu and S. Flach, Phys. Rev. Lett. **113**, 236403 (2014).
  - [25] We have varied this cutoff value up to  $\xi \leq N$ , and it does not change the spectra drastically.
  - [26] With a similar argument discussed in Sec.III, in this antisymmetry all the eigenstates are expelled from the flat-band energy  $E = t$ .
  - [27] L.A. Ponomarenko, A. K. Geim, A. A. Zhukov, R. Jalil, S. V. Morozov, K.S. Novoselov, I. V. Grigorieva, et al., Nat. Phys. **7**, 958 (2011).
  - [28] B. Radisavljevic and A. Kis, Nat. Mat. **12**, 815 (2013).
  - [29] J. Givernaude, C. Champeaux, A. Catherinot, A. Pothier, P. Blondy, and A. Crunteanu, IEEE MTT-S Intl., 1103 (2008); F. Fan, Y. Hou, Z. Jiang, X. Wang, and S. Chang, Appl. Opt. **51**, 4589 (2012).